Dextran Functionalized Surfaces via Reductive Amination: Morphology, Wetting, and Adhesion

Davide Miksa,[†] Elizabeth R. Irish,[‡] Dwayne Chen,[†] Russell J. Composto,[‡,§] and David M. Eckmann*[,†,§,||]

Departments of Anesthesiology and Critical Care and Material Science and Engineering, Institute for Medicine and Engineering, and Institute for Translational Medicine and Therapeutics, University of Pennsylvania, Philadelphia, Pennsylvania 19104

Received August 21, 2005; Revised Manuscript Received November 27, 2005

Dextran surface grafting density was systematically varied via a two-step process involving SiO_2 amination by aminopropyltriethoxy silane (APTES) followed by oxidized dextran (M_w = 110 kDa) chemisorption. Dextran oxidation kinetics with sodium metaperiodate ($NaIO_4$) were quantified by ^1H NMR and pH measurements. Aldehyde group formation increased with increasing oxidation time. For 0.5 h oxidation time, dried film ellipsometric thickness was constant for solution concentrations ranging from 1 to 4 mg/mL. Dextran layers with the lowest grafting density wetted fastest and displayed the lowest contact angle ($\theta_{APTES} > \theta_{1h} > \theta_{2,4h} > \theta_{0.5h}$). Under aqueous conditions, AFM force versus displacement measurements on 0.5 and 4.0 h surfaces exhibited a single displacement jump upon retraction. The 1.0 and 2.0 h surfaces showed two jumps consistent with two populations of chains, namely, loosely and strongly bound dextran. Overall, film morphology and wetting behavior were relatively invariant with grafting density, confirming the method's robustness for preparing biomimetic coatings with consistent properties.

Introduction

Increasing demands to control biochemical interactions at the tissue/material interface have prompted scientists to investigate polysaccharides and proteoglycans, native components of the glycocalyx,[1] as coatings for biomaterials.[2−4] Although some understanding of such coatings exists, the wettability and spatial organization at the biomaterial surface are still recognized as the limiting factors in biocompatibility.[5] Therefore, new surface synthetic approaches that will afford reproducible control over the surface morphology of the biomaterial coating are of great interest. Furthermore, surface characterization must be performed with the resolution and under conditions consistent with the working environment of the biomaterial so that performance can be directly attributed to the structural and functional properties of the coating. Because increased surface roughness can promote protein adhesive as well as micro-embolic events, smooth silicon wafers with a SiO_2 surface layer were chosen as model substrates for subsequent modification. Although not a biomaterial per se, silicon wafers have the advance of reliable and reproducible surface modification and lend themselves to rigorous characterization techniques. Organosilane self-assembled monolayers (SAMs)[6] were used to produce an amine-functionalized SiO_2 surface (SiO_2 + APTES) onto which oxidized dextran was immobilized via reductive amination. Some elements of these studies were presented at the 228th meeting of the American Chemical Society (Philadelphia, August 22−26, 2004). This two-step modification procedure is highly versatile, because SAMs can be applied to a wide range of biomaterials, such as titanium and poly(dimethylsiloxane).

The objectives of this study were to prepare dextran coatings with varying grafting densities and to ascertain whether controlling the grafting density would produce significant changes in relevant film properties such as morphology and wetting. For these reasons, atomic force microscopy (AFM) and water (H_2O) contact angle goniometry were the primary characterization tools. Tapping-mode AFM has been established as a nondestructive method to characterize the morphology of biofilms.[7,8] AFM was used to show that all films were relatively smooth with similar rms roughness values, about 2.0 nm. However, the morphology of dextran layers prepared with intermediate oxidation times (1 and 2 h) were determined to be different from those prepared from short (0.5 h) and long (4 h) oxidation times. By measuring the force versus displacement behavior, AFM can also be used to probe the adhesive forces generated between the tip and the dextran coating as well as between the coating and the substrate. These measurements suggest that the large features at intermediate times are due to two populations of dextran, those molecules covalently grafted and therefore more strongly bound to the substrate and molecules weakly bound via nonspecific interactions, such as electrostatic ones, between free ammonium groups on the surface and negatively charged dextran.

Experimental Section

Materials and Methods. All reagents and solvents were used as received unless otherwise stated. (Aminopropyl)triethoxysilane (APTES), sodium periodate, 99% ($NaIO_4$), sodium cyanoborohydrate ($NaBH_3$-CN), and dimethylformamide were purchased from Sigma-Aldrich Co. Dextran prepared from Leuconostoc ssp (Mw = 110 000, Mw/Mn = 1.52) was supplied by Fluka Chemie. Deuterium oxide (D_2O, 99.9%) for ^1H NMR was obtained from Cambridge Isotope Laboratories, Inc.

* To whom correspondence should be addressed at the Department of Anesthesiology and Critical Care, 331 John Morgan Building, University of Pennsylvania, Philadelphia, PA 19104. E-mail: EckmannDM@uphs.upenn.edu.

[†] Department of Anesthesiology and Critical Care.

[‡] Department of Material Science and Engineering.

[§] Institute for Medicine and Engineering.

[||] Institute for Translational Medicine and Therapeutics.

10.1021/bm050601o CCC: $33.50
Published on Web 12/27/2005

Table 1. Ellipsometric Thickness (Å), Rate of Wetting (k_W), and Force of Adhesion (F_{adh}) for SiO_2, APTES, and Surfaces Grafted with Dextran Oxidized for 0.5−24 h

surface	thickness[a] (Å)	$k_W \times 10^3$ (s^{-1})	F_{adh}[b] (nN)[b]
SiO_2	21 ± 1.0	NA	0
APTES	5.0 ± 1.0	2.8	3.0 ± 1.0
0.5 h Dextran	5.0 ± 3.0	3.5	2.0 ± 1.0
1.0 h Dextran	3.0 ± 2.0	2.5	2.0 ± 1.0
2.0 h Dextran	2.0 ± 1.0	2.8	5.0 ± 2.0
4.0 h Dextran	2.0 ± 2.0	3.2	2.0 ± 1.0
24.0 h Dextran	97.3 ± 1.7	NA	NA

[a] Dry. [b] Aqueous.

H_2SO_4 (96% by assay) and H_2O_2 (30% by assay) were obtained from Fisher Scientific. Finally, silicon oxide surfaces (⟨1−0−0⟩, $R = 1-5$ Ω cm) were purchased from Silicon Quest International (Santa Clara, CA). In all cases, the water came from a Millipore filtration system and had a resistivity of 18.2 mΩ. The extent of dextran oxidation was quantified by ^{1}H NMR spectroscopy (Bruker, 250 MHz) via in situ monitoring of HCO_2H production. The NMR results were confirmed by pH measurements (Denver Instruments model 250 meter and pH/ATC electrode) conducted at room temperature over 22 h at 30 min intervals.

APTES Surface Preparation. Silicon surfaces (3.0 cm × 4.5 cm) were etched clean by immersion in "piranha" solution (70% H_2SO_4 and 30% H_2O_2, v/v) for 20 min. at 80 °C, washed with copious amounts of water, and then soaked overnight in water. Afterward, the surfaces were dried with compressed N_2(g) and exposed to ultraviolet light in a UVO−Cleaner model 144A (Jelight Company, Inc.; Irvine, CA) for 20 min. This procedure resulted in a homogeneous silanol layer that could react with APTES deposited by vapor deposition under inert atmosphere in a glovebox. A cylindrical glass jar, 9 cm high by 7 cm wide, was the reaction vessel for the APTES deposition. The APTES (2 mL) was transferred into the jar using a graduated syringe. A freshly prepared silicon substrate was then laid face down on a 2-cm-high glass ring within the glass jar. The vessel was then sealed with Para film and heated at 80 °C for 1 h in a fume hood. At these conditions, the silicon was exposed to an APTES vapor pressure of 4.01 Torr.[9] The APTES modified surfaces were characterized by ATR-FTIR (not shown). After repeated sonication in water, the presence of adsorption bands at 3266 cm^{-1} (ν_{N-H})[10] and 1590 cm^{-1} (δ_{N-H})[11] is representative of primary amines and is consistent with covalently bonded APTES on silicon.

Dextran Surface Immobilization. The $NaIO_4$ oxidation of glucose as a facile route to aldehyde functionalization has long been established,[12] while Dai et al.[2] have successfully immobilized oxidized dextran onto polymer surfaces exposed to *n*-heptylamine gas plasma. Building on these findings, the present work varied the extent of dextran oxidation in an attempt to control the grafting density of dextran on APTES using the follow method. First, 100 mL of aqueous dextran solution (1 mg/mL) was partitioned into five 20 mL aliquots, one for each oxidation time plus one spare. Next, the amount of $NaBH_3CN$ corresponding to 1.5 times the stoichiometric amount of $NaIO_4$ in the reaction was weighed into four separate 50 mL beakers under anhydrous conditions. After the appropriate oxidation time, the dextran solutions were transferred to the 50 mL beakers containing $NaBH_3CN$. After immediate mixing, these solutions were transferred to Petri dishes containing APTES modified silicon wafers. The Petri dishes were then left overnight on an orbital shaker. After the dextran immobilization time had elapsed, the wafers were removed from solution, washed with copious amounts of water, and sonicated in water for 30 min. The consistency in film thickness (Table 1) and contact angle measurements for dextran-modified surfaces were taken as proof of the reproducibility and robustness of the reductive amination reaction as a synthetic route to covalently bind aldehyde-functionalized macromolecules onto amine-terminated surfaces. Further support is found in the literature.[13,14] For short oxidation times, the dextran can only covalently graft by a few

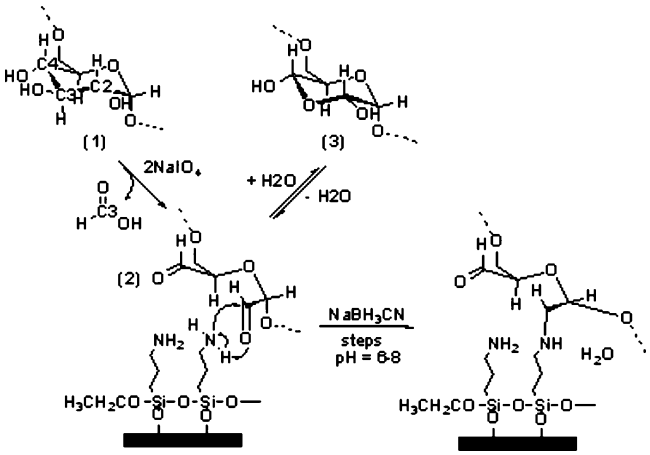

Figure 1. Reaction scheme for the oxidation of dextran glucopyranoside subunits by $NaIO_4$ with formation of formic acid, HCO_2H, and subsequent surface immobilization via reductive amination in the presence of $NaBH_3CN$. The substrate is silicon oxide, which reacts with APTES to provide $-NH_2$ functionalized surfaces.

subunits, resulting in a highly extended brush in good solvent (i.e., water), whereas long oxidation times would result in a tightly bound molecule. A brief summary of the dextran oxidation chemistry follows. The oxidation of the anhydroglucopyranoside (**1**) (Figure 1) subunits by $NaIO_4$ produced the dialdehyde in (**2**) as well as formic acid. The reaction proceeded via the formation of two subsequent cyclic periodate esters and therefore required 2 mol of $NaIO_4$ per mole of (**1**). The first ester was formed by the nucleophilic attack of the vicinal hydroxyls of carbons C2, C3, or C4 on the iodine of the first IO_4^-. The important step of the reaction was the bond breaking between the hydroxyl-bearing carbons. The first bond cleavage produced a dialdehyde one carbon longer than (**2**) with a remaining hydroxyl group. The second ester was formed by the nucleophilic attack of the remaining hydroxyl and one of the aldehyde oxygens. The subsequent C−C bond cleavage produced the final dialdehyde, (**2**), and formic acid. Finally, (**2**), which is in equilibrium with its cyclic hydrate (**3**), underwent reductive amination upon exposure to the APTES modified silicon substrates in the presence of $NaBH_3CN$. As a result, stable covalent bonds were formed between dextran and the substrate.

Atomic Force Microscopy. All surfaces were analyzed by atomic force microscopy (AFM) under aqueous conditions using Si_3N_4 probes (spring constant = 0.06 N/m for imaging, 0.32 N/m for force measurements) with reference to work by Lo et al.,[15] Dupont-Gillian et al.,[16] and Morra et al.[17] All imaging scans (tapping mode) as well as force of adhesion (F_{adh}) measurements were performed with a DI Multimode AFM scanning probe microscope (Veeco Metrology, Chadds Ford, PA). A liquid cell was employed for scans under aqueous conditions. Following Lo et al.,[15] who studied the contamination of commercial cantilevers, Si_3N_4 probes were cleaned by immersion (∼30 s) in "piranha" solution (70% H_2SO_4, 30% H_2O_2, v/v), rinsed with copious amounts of water, air-dried, and then exposed to UV light for 15 min, as per manufacturer's suggestion.[18] This cleaning procedure most likely resulted in a combination of primarily silanol and some silylamine groups being formed on the surface of the AFM probe. Since the present force of adhesion measurements were conducted under aqueous (Millipore, 18.2 mΩ) conditions, the electrostatic contribution to the tip/surface interaction could not be ignored. The extent of such interaction, which is a complex function of pH, van der Waals forces, and chemical species involved, cannot be easily quantified.[19] It is, however, reasonable to assume that it is regulated by an acid−base (i.e., donor−acceptor) mechanism. Therefore, the force of adhesion data herein presented were collected only after the probe/surface interaction had reached equilibrium, as evidenced by unchanging force−distance curves. In so doing, the electrostatic contribution was brought to a steady state, and therefore considered constant throughout the analysis. Furthermore, since the same AFM probe was used in the analysis of

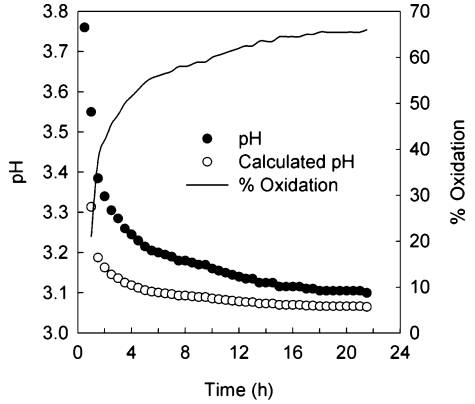

Figure 2. Measured (●) and calculated (○) pH values for the $NaIO_4$ oxidation of dextran. The data were measured at room temperature every 30 min over 22.0 h. The average difference between the experimental and calculated values is 2.3%. The percent oxidation was based on eq 1, namely, production of formic acid during oxidation.

all surfaces, the nominal cantilever spring constant of 0.32 N/m provided by the manufacturer (Veeco Metrology) can be considered a global constant. Imaging scans were acquired at probe velocities of 4 μm/s (10 × 10 μm^2) and 2 μm/s (1 × 1 μm^2). Furthermore, image optimization was achieved by increasing the amplitude setpoint until the probe was fully retracted. Then, the setpoint was reduced in small increments until the probe re-engaged the surface. This procedure ensured minimum tip−sample forces, and therefore, tip-induced artifacts were avoided. Force of adhesion measurements were performed in contact mode under aqueous conditions. The scan size was set to zero prior to the engagement of the tip onto the surface. The scan rate was 0.5 Hz, and the scan length was 1.0 μm. Five force of adhesion measurements (i.e., curves) were collected on five separate locations of each surface, resulting in a total of 25 measurements per oxidation time.

Scanning Electron Microscopy. The Si_3N_4 probes used in the AFM analysis were imaged and analyzed by scanning electron microscopy (SEM) using a Joel 6400 scanning electron microscope (Peabody, MA). For some cases, probes were sputter-coated with Au to reduce charging. Energy-dispersive X-ray spectra (EDS) were also collected (10 kV, 230 s) to identify and map the elements including Si, O, N, and C.

Contact Angle. Using a 1 μL sessile drop, water contact angle measurements were performed at room temperature and humidity conditions. The analysis was performed with a Ramé-Hart (Mountain Lakes, NJ) model 100-00 goniometer with a software-controlled auto-pipetting system and the DROPimage advanced software package. The contact angle was determined by a numerical curve fit of the droplet profile at the three-phase boundary as captured by a CCD camera. Advancing/receding measurements were conducted at room conditions by varying the volume of the H_2O drop, initially at 1 μL, from 2 to 5 μL in 1 μL increments over 60 s. Data were collected between 1 and 5 min at 5 s intervals and resulted from measurements of at least three drops on at least three different regions for each sample. After each advancing and receding step, a five second relaxation period (data not shown) was allowed prior to the next volume change. Room-temperature relaxation measurements were conducted over a 1 min. time period to avoid evaporation. The drop had not reached equilibrium within 1 min on any surface. The analysis time did not exceed 5 min.

Results and Discussion

Dextran Oxidation and Grafting. Dextran coatings were prepared by a two-step process involving the oxidation of dextran followed by dextran grafting to aminated silicon. The grafting density was controlled by varying the concentration of aldehyde subunits (i.e., potential attachment points) along the dextran backbone. The $NaIO_4$ oxidation chemistry of dextran (eq 1) was followed by in situ ^1H NMR and pH measurements.[12] Both techniques measured the production of formic acid (HCO_2H) by following either an increase in the aldehyde proton shift of HCO_2H (8.26 ppm) or a decrease in the pH of the solution. Over 22 h, the percent change between subsequent pH values was used to calculate the percent of dextran oxidation based on the formation of HCO_2H (see Figure 2).

$$(C_6O_5H_{10})_n + 2IO_4^- + H_2O \xrightarrow{k_{ox}} (C_5O_4H_6)_n + HCO_2H + 2H_2IO_4^- \quad (1)$$

To determine whether the pH values were solely determined by the HCO_2H dissociation equilibrium (eq 2), a theoretical pH profile was obtained from the rearranged dissociation equilibrium expression of HCO_2H (eq 3).

$$HCO_2H + H_2O \overset{K_a}{\longleftrightarrow} HCO_2^- + H_3O^+ \quad (2)$$

$$K_a = \frac{[H_3O^+][HCO_2^-]}{[HCO_2H]} = \frac{[H_3O^+]^2}{[HCO_2H]}$$

$$[H_3O^+]_t = \sqrt{K_a[HCO_2H]_t} \quad (3)$$

in which

$$[HCO_2H]_t = [(C_6O_5H_{10})_n]_0 \times \{(pH_{ti} - pH_{ti+1}) \times 100\} \quad (4)$$

By using the initial dextran concentration, $[(C_6O_5H_{10})_n]_0$, to determine the amount of HCO_2H produced at a given time, the pH can be independently determined from the amount of oxidized dextran. Figure 2 shows that both the calculated and the experimental pH values decrease exponentially during the early stages of the oxidation, 0.5−4 h, and then approach a pH of 3.1 after 22 h. The initial rapid decrease in pH indicates that the oxidation of dextran by $NaIO_4$ is rapid, reaching completion after about 15 h. The calculated pH was an average of 2.3% less than the experimental values, with the largest difference occurring during the early stage, i.e., 0.5−8 h. To account for this difference, the equilibria associated with the meta-periodate ion in water (eqs 5−7) were also considered in calculating the pH values[20−22]

$$H_4IO_6^- \overset{K_D}{\longleftrightarrow} IO_4^- + 2H_2O \quad (5)$$

$$H_5IO_6 \overset{K_1}{\longleftrightarrow} H_4IO_6^- + H^+ \quad (6)$$

$$H_4IO_6^- \overset{K_2}{\longleftrightarrow} H^+ + H_3IO_6^{2-} \quad (7)$$

The amount of IO_4^- lost to the hydration reaction described by equilibrium 5 (reverse reaction) was calculated using $1/K_D$ as the equilibrium constant, where $K_D = 40.74$.[22] Using this constant to determine $[H_4IO_6^-]$, $[H_5IO_6]$ can be calculated from the reverse reaction of equilibrium 6, where $K_1 = 0.000\,501$.[22] Equilibrium 7 is not a factor, because $K_2 = 2.04 \times 10^{-7}$.[22] Because H^+ is consumed, the reverse reaction of equilibrium 6 is the only one that could account for the higher experimental pH values. However, including this correction to $[H^+]_t$ does not change the calculated pH values significantly. This observation confirms that the IO_4^- equilibria (eqs 5−7) do not affect the overall pH of the solution and that the disparity between the calculated and experimental pH values most likely results from instrument and operator error.

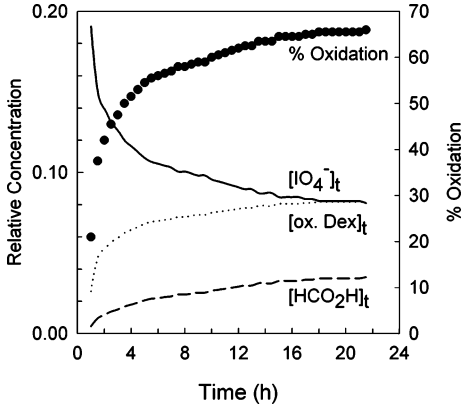

Figure 3. Concentration of oxidized dextran (dotted line) and formic acid (dashed line) as a function of oxidation time. The concentration of IO_4^- (solid line) decreases at the same rate as the oxidized dextran and formic acid increase in agreement with the proposed reaction scheme. The percent oxidation of dextran (●) is taken from Figure 2.

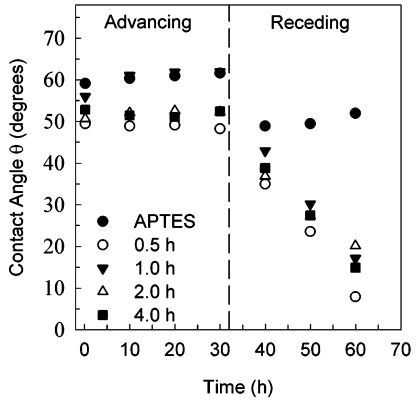

Figure 4. Dynamic contact angles for water on APTES and dextran grafted surfaces. Using 1 μL increments, the drop volume increased from 2 to 5 μL during advancement and decreased from 5 to 2 μL during recession. As the water advanced across the surface, the area of the drop increased from 4.3 to 8.6 mm^2.

Figure 3 shows how $[IO_4^-]_t$, determined from eqs 5−7, oxidized dextran or $[\text{ox. dex.}]_t$, and formic acid or $[HCO_2H]_t$ vary with oxidation time. The $[IO_4^-]_t$ profile initially decreases rapidly and then approaches a constant value after approximately 16 h, in agreement with the pH behavior in Figure 2 (vide supra). Furthermore, the $[IO_4^-]_t$ values were corrected for the amount of IO_4^- lost to $H_4IO_6^-$ because of the hydration reaction described by equilibrium 5. This amount was ∼2.5% of the initial IO_4^- concentration. The concentration of oxidized dextran shown in Figure 3 mirrors the $[IO_4^-]_t$ data, and is consistent with a 2:1 ratio between IO_4^- and dextran (eq 1). Although the amount of oxidized dextran and formic acid produced have identical stoichiometries (i.e., 1:1 ratio, eq 1), Figure 3 shows that $[HCO_2H]_t$ is lower than $[\text{ox. dex.}]_t$. It is important to note that the $[HCO_2H]_t$ data do not represent the total HCO_2H produced by the oxidation of dextran, but rather the amount that is in equilibrium with its conjugate base (eq 2). Therefore, the difference between $[HCO_2H]_t$ and $[\text{ox. dex.}]_t$ is the amount of HCO_2^- produced according to the dissociation equilibrium of HCO_2H.

The percent oxidation of dextran shown in Figures 2 and 3 is important, because it determines the maximum possible grafting density of dextran, which is the number of attachment points that dextran could theoretically have with APTES if all the aldehyde groups reacted with all the available $-NH_2$ moieties. A direct measure of the reacted $-NH_2$ groups by either FTIR or NMR was beyond the scope of this study. Rather, an indirect measure of the dextran grafting density can be obtained by analyzing the morphology of the grafted layer by AFM as shown later in Figure 5. Although a direct comparison between percent oxidation and film morphology is not possible, a qualitative comparison is meaningful and consistent with starting hypotheses. Namely, at low oxidation (i.e., 0.5 h), *individual* dextran molecules form relatively few bonds with surface sites, because the number of oxidized glucopyranoside subunits per molecule is low. Because molecules are strongly hydrated and extend away from the substrate (i.e., polymer brush), many dextran molecules are able to access the surface sites to produce a high grafting density of molecules per surface area. As percent oxidation increases, many surface sites react with a single molecule resulting in a more tightly bound molecule and a lower grafting density. A premise of this paper is that an increase in dextran oxidation (e.g., Figures 2 and 3) will decrease the grafting density of molecules (i.e., one molecule takes up more surface sites). The precise relationship is rather complicated because of mutual repulsion between the slightly negatively charged glucopyranoside subunits, which tend to expand the molecule, as well as possible attractive interactions between these subunits and the substrate. Further studies using salts to screen the repulsive interactions between molecules are worth pursuing.

Wetting. Figure 4 shows the advancing and receding H_2O contact angles under ambient conditions for the APTES and dextran grafted surfaces. The advancing contact angle on APTES (θ^{ad}_{APTES}) was 60.5 ± 1.1°, in good agreement with published values for both solution[23] and vapor[24] deposited APTES. For the dextran surfaces prepared from 0.5, 2.0, and 4.0 h oxidation times, the θ^{ad} values were similar, 49−53°, whereas the 1.0 h case displayed θ^{ad} values similar to APTES. This latter behavior may be attributed to exposed APTES as noted in a subsequent section (vide infra). Finally, as the H_2O volume, and therefore area, of the drop increased from 2 to 5 μL (4.3−8.6 mm^2), the advancing contact angle values for all dextran grafted surfaces remained within 2° of the preceding value. This consistency in advancing angles suggests a uniform coverage of dextran.

For dextran grafted surfaces, the receding contact angle (θ^{re}) values were less than θ^{ad}, and their difference, $|\theta^{adv} - \theta^{re}|$, represents the contact angle hysteresis. In general, hysteresis can be attributed to surface roughness, surface heterogeneity, solution impurities, or molecular rearrangements due to the liquid droplet. Because dextran is readily hydrated by water, the molecular rearrangements, as pointed out by Andrade[25] and Holly et al.,[26] can occur to minimize the interfacial tension between the water droplet and dextran. Figure 4 shows that the hysteresis of dextran surfaces is greater than that of APTES, consistent with dextran molecules undergoing conformational changes upon hydration. Conformational freedom is expected to depend on the number of anchoring points which determines the "loop" length between anchors. However, a systematic trend with increasing oxidation is not observed. Qualitatively, the similar hysteresis values for the 0.5, 2, and 4 h samples are consistent with their similar morphology. As described later (cf., Figure 5), these samples do indeed display a similar number of 5 nm features.

In contrast to θ^{ad}, Figure 4 shows that θ^{re}_{dex} decreased strongly with time as the H_2O drop receded back to its original volume on the dextranized surfaces. In contrast, θ^{re}_{APTES} remained constant, 50.1 ± 1.6°, consistent with a smooth, homogeneous surface that remains unaltered by the water droplet. Because θ^{re}_{dex} decreased on dextran grafted surfaces,

$|\theta_{dex}^{adv} - \theta_{dex}^{re}|$ also increased as contact time increased. This behavior is consistent with the rearrangement of dextran molecules during the time of contact between the water droplet and the dextran. Because each advancing and receding measurement was 30 s in duration, the initial contact area on the dextran surface was hydrated the longest. Therefore, the grafted dextran chains in this area had the longest time to rearrange and adopt a conformation that minimized the interfacial tension, which, in turn, resulted in a decrease of θ_{dex}^{re}. This observation demonstrates that the kinetics of hydration can be extremely rapid and that molecular rearrangements can occur within 1 min under ambient conditions.

Further, to understand wetting kinetics, contact angles, θ, were measured over 60 min using constant volume drops on all surfaces. Within experimental limits, complete wetting (contact angle $< 5°$) was observed for the freshly prepared SiO_2 and dextran grafted surfaces prepared from the 24.0 h oxidized dextran. The rate of wetting (k_W) was determined from the slope of ln θ versus time and is summarized in Table 1. No clear trend is observed with increasing oxidation time. However, the rate of wetting was consistently faster on the 0.5 h surface (i.e., lowest grafting density). This observation may suggest that the loops between grafting points can quickly rearrange upon hydration.

In recent years, Sackmann and co-workers have prepared and characterized thin hydrated dextran films on silanized substrates. Although the details of their approach differ from those in this paper, the properties of the dextranized films from our work are in general agreement with those of Sackmann and colleagues.[27,28] They report a mean thickness of 3.9 ± 1.1 Å for dextran covalently attached onto silanized glass prepared by the vapor deposition of 4-aminobutyldimethylmonomethoxy silane (ADMS). Although this silane contains a butyl link instead of the propyl in APTES, the thicknesses of ADMS and APTES are consistent (see Table 1). In their studies, the advancing contact angle of dextran was $\theta^{ad} = 55°$, in agreement with the value of $\theta^{ad} = 60.5°$ reported in this present work.

The properties of dextran functionalized surfaces in the present paper are also consistent with earlier work by Kuhner et al.[27] who immobilized 500 kDa dextran onto 3-glycidyloxypropyltrimethoxy (GOPTS) silanized substrates. After a 24 h incubation of the GOPTS functionalized substrates in a 300 mg/mL dextran solution, dextran layers with an average thickness of 101.6 ± 5.2 nm were produced. Although their approach uses an organosilane with a different endgroup and much greater dextran concentrations, the thickness of dextran is similar to our study at the same immobilization time (i.e., 24.0 h). As indicated in Table 1, we find a thickness of 97.3 ± 1.7 Å upon incubating APTES functionalized SiO_2 in solutions containing 110 kDa dextran oxidized for 24 h. Because our procedure and that of Kuhner et al.[27] produce dextran coatings with similar properties, despite differences in specific conditions and materials, dextran immobilization via reductive amination represents a robust methodology for the controlled biofunctionalization of organo-reactive substrates.

Morphology. Figure 5 displays representative topography scans of the dextran grafted surfaces over an area of 10 μm × 10 μm. In all cases, dextran features are uniformly distributed across the substrate. Two-dimensional AFM imaging scans were used to characterize the height, surface roughness, diameter, and density of dextran features over an area of 100 μm^2. For noncircular features, the diameter was calculated from an equivalent circle having the same area as the real feature. The data are given in Table 2. Note that the height, ~5 nm, and the root-mean-square (rms) roughness, ~2 nm, did not change appreciably with increasing oxidation time. The diameter and the density of dextran features, however, displayed different trends as the oxidation time was increased. The diameter increased as the oxidation time increased from 0.5 to 1.0 h and then gradually decreased with time (i.e., 2.0 and 4.0 h). The density of dextran molecules per area, on the other hand, decreased after 0.5 h of oxidation, and moderately from 1.0 to 2.0 h. After 4.0 h, the density increased to a value similar to the 1.0 h case. Comparison of the rms roughness and the diameter values revealed a repeating trend whereby the shortest, 0.5 h, and longest, 4.0 h, oxidation times resulted in surfaces having similar characteristics.

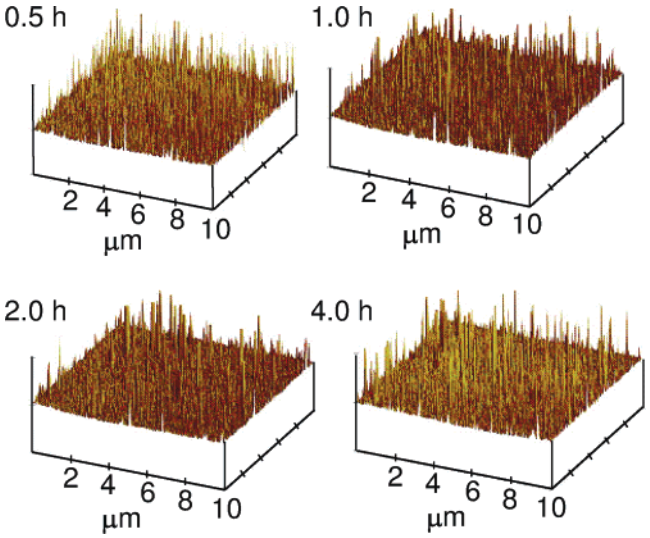

Figure 5. Aqueous AFM topography scans for dextran grafted surfaces (Z scale = 20 nm). The scans were collected in tapping mode using a Si_3N_4 cantilever. The rms roughness as well as feature density, diameter, and height are given in Table 2. The xy scan size is 10 × 10 μm^2.

Table 2. Comparison of the RMS Roughness, Height, Diameter, and Density of Dextran Features as a Function of Dextran Oxidation Time

oxidation time (h)	roughness (nm)	height (nm)	diameter (nm)	density ($/\mu m^2$)
0.5	1.7 ± 0.5	5.4 ± 5.7	48.5 ± 33.5	26.8
1	1.4 ± 0.3	4.8 ± 3.6	59.4 ± 35.6	14.9
2	1.2 ± 0.5	4.3 ± 3.8	52.5 ± 35.2	13.3
4	1.9 ± 0.8	5.0 ± 5.3	48.6 ± 37.4	16.6

Before attempting to rationalize the trends in feature characteristics, it is important to note that all dextran modified surfaces were prepared from 1 mg/mL dextran solutions. This concentration was well below the overlap limit, c^*, which for 110 kDa dextran was 20−29 mg/mL according to Catalina et al.[29] and Hirata et al.[30] Furthermore, the radius of gyration, R_g, for this molecular weight is 9−12 nm.[29,30] Therefore, the mechanism of attachment is most likely consistent with the scheme in Figure 1, namely, that the features form when the oxidized dextran from solution interacts with the surface-bound dextran, as opposed to free dextran chains aggregating in solution and subsequently reacting with the SiO_2 + APTES substrate. This assumption is critical if the surface parameter data are interpreted in terms of the dynamics of the dextran layer.

Although the data do not support a direct connection between the dextran oxidation time and the surface features observed

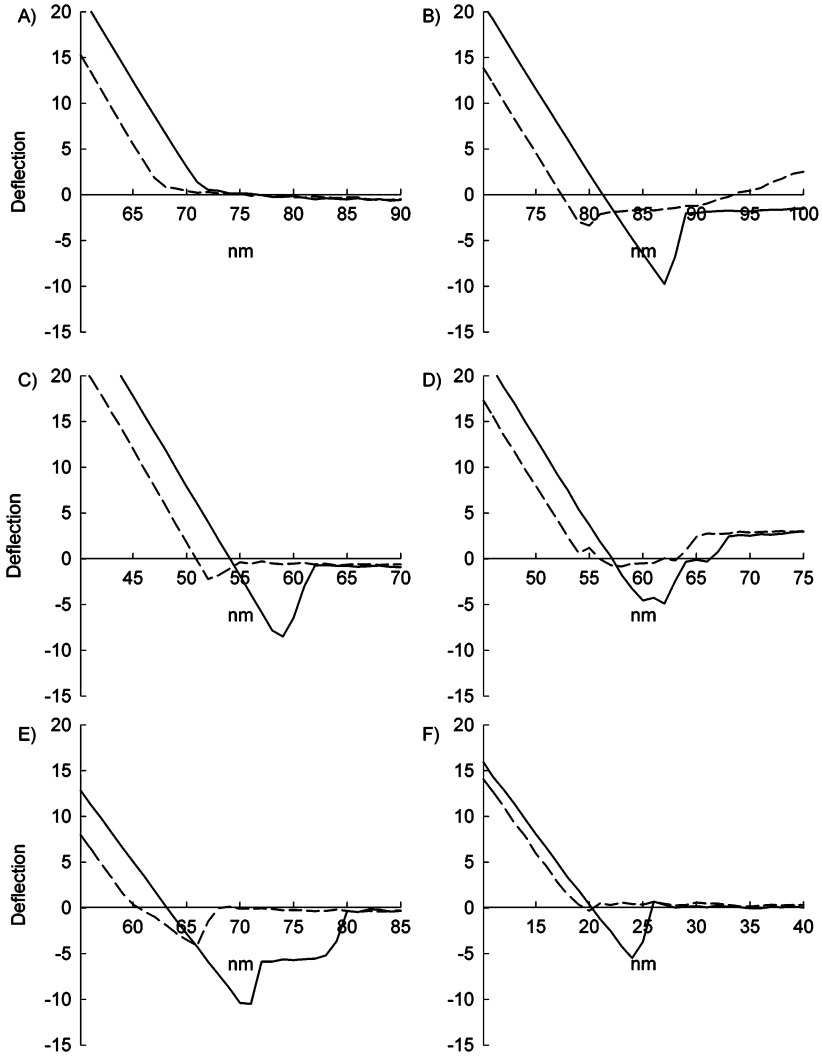

Figure 6. Representative tip−sample separation curves for force measurements between a Si_3N_4 tip and surfaces under aqueous conditions. The cantilever was held static as the surface was oscillated by an amplitude of 1 μm at a frequency of 0.5 Hz. The surface and cantilever were allowed to reach equilibrium prior to the measurement. The approach trace is the dashed line in each panel. Surfaces were as follows: (A) SiO_2; (B) APTES; (C) dextran, 0.5 h; (D) dextran, 1.0 h; (E) dextran, 2.0 h, and (F) dextran, 4.0 h.

by AFM, it is still informative to make tentative correlations. The morphology changes observed in the images of Figure 5 are qualitatively consistent with an increasing grafting density on a per molecule basis associated with increasing oxidation time. Recall that, as the extent of oxidation was increased, more glucopyranoside subunits of dextran were converted to dialdehydes (see Figure 1), which then reacted with APTES to produce a more tightly bound dextran layer with a low grafting density of dextran molecules on a per area basis. It is reasonable to assume that a more tightly bound dextran layer would result in a continuous surface with fewer asperities. Therefore, as the oxidation time, and consequently the number of possible bonds to APTES, was increased, the resulting dextran layers should have been more continuous and thicker. This, however, was not observed entirely. If we consider the density of dextran features to be a relative measure of the continuity of the dextran layer, then the surface corresponding to the shortest oxidation time, 0.5 h, resulted in the highest density of dextran features, as expected. The feature density for the remaining surfaces (1.0, 2.0, and 4.0 h), however, did not vary appreciably, as noted in Table 2. Furthermore, the height of the dextran features did not change significantly for all surfaces. This leads us to believe that varying the oxidation time of dextran in the 0.5−4.0 h time range did not affect the surface morphology in the *z* direction (i.e., height) but rather in the *xy* plane. This point is partially supported by the values recorded for feature diameters. As the oxidation times were increased from 0.5 to 1.0 h, the feature diameters increased by 18%, indicating, as expected, a greater (i.e., more continuous) coverage of the dextran layer. The remaining surfaces, 2.0 and 4.0 h, exhibited feature diameters similar to those of the 0.5 and 1.0 h surfaces, respectively, which cannot be rationalized with the present interpretation. Overall, we find that, with the exception of the feature density, the morphology of the dextran surfaces did not vary significantly. We take this to be an indication of the robustness of the grafting chemistry used in preparing these surfaces. This behavior is consistent with the decrease in density of dextran features with increasing oxidation time noted in Table 2. However, as the oxidation time increased, feature height remained relatively constant, whereas the density decreased and the feature diameter increased. These observations suggest that the grafted dextran chains occupy a greater surface area as the oxidation time, and therefore the number of possible covalent bonds, is increased. Such increase in area of coverage would result in wider dextran

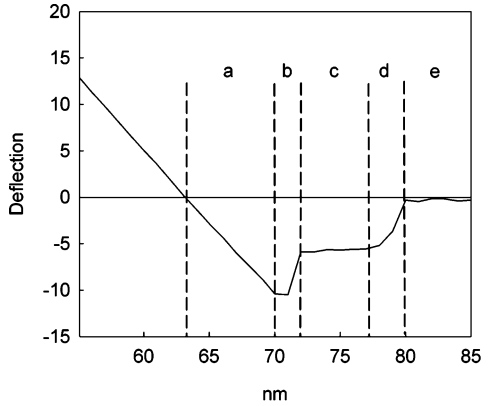

Figure 7. Representative retraction trace for the 2.0 h dextran surface obtained by AFM with a Si_3N_4 cantilever under aqueous conditions. The trace can be divided in the following segments: (a) Deflection of cantilever due to initial adhesion onto unperturbed dextran layer, 13.3 nm. (b) Pulling off of dextran feature from surface. At this point the dextran polymer is still coiled and connected to both the cantilever tip and the surface, 2 nm. (c) Stretching of dextran coil as surface is retracting from cantilever. The cantilever does not move during the uncoiling as evidenced by the plateau, 11.7 nm. (d) Fully elongated dextran polymer snaps, disconnecting the cantilever tip from the retracting surface, 4 nm. (e) Initial equilibrium position of cantilever.

features (i.e., larger diameter) while not affecting the height of the features significantly. Furthermore, because of the increase in the base of the features, fewer could form over the 100 μm^2 area of interest. Consequently, the density of dextran features would appear to decrease. This interpretation seems valid up to the 4.0 h oxidation point. As mentioned earlier, this surface behaved similarly to the 0.5 h surface. Although the present data is not conclusive, an explanation consistent with the previous interpretation is that, at some point between 2.0 and 4.0 h of oxidation, the SiO_2 + APTES substrate was no longer accessible to the oxidized dextran. In the case of the 4.0 h surface, this resulted in interchain conglomeration between the solution and the surface-bound dextran, whereby the 4.0 h point marked the onset of a multilayer dextran surface. This interpretation is further substantiated by surfaces prepared using dextran oxidized for 24 h (see Table 1) where the ellipsometric thickness values were a clear indication of a multilayer scenario.

Adhesion Measurements. To probe the compliance and the force of interaction, force of adhesion (F_{adh}) measurements were conducted on the dextran layer under the same conditions as the AFM experiments. The data are shown in Figures 6 and 7, which summarize the qualitative as well as quantitative (F_{adh} values, Table 1) aspects of the measurement. Representative force−distance curves in Figure 6 readily show the differences in the extent and the nature of the forces of interaction between the AFM probe and the different samples. The two traces correspond to the approach of the sample surface toward the stationary AFM probe and the retraction of the surface from the probe. As expected for a hard substrate, the force−distance curves for the unmodified SiO_2 surface did not record any jump to contact during the approach step or deflection during the retraction step. This lack of interaction between probe and SiO_2 surface confirmed the validity of the cleaning procedure suggested by Lo et al.[11] Furthermore, the absence of any attraction between the sample and the probe supports the assumption that silanol groups comprise the AFM probe primarily as a result of the cleaning procedure. In the case of the APTES modified SiO_2, the force−distance curve revealed substantial attractive forces. The main component of these attractive forces is most likely the donor−acceptor interaction between the −OH terminated AFM probe surface and the $-NH_2$ of the APTES.

The dextran modified surfaces exhibited force−distance curves that depended on oxidation time. In particular, the 0.5 and 4.0 h surfaces showed single pullout deflections, whereas the 1.0 and 2.0 h surfaces exhibited multistep pullout profiles. Although the force−distance curves shown for these two surfaces are statistically representative, a unique physical interpretation is difficult. However, one can speculate about the origin of the features in a manner consistent with the morphology of the dextran. The larger feature diameters associated with the 1.0 and 2.0 h oxidation times may result from loosely noncovalently bound dextran molecules. The origin of the loosely bound dextran can be explained by interchain entanglement between the "loops" of the covalently bound dextran and loosely bound, extended dextran. We hypothesize that these extended, trapped molecules can be partially detached by the retracting AFM probe. Prior to complete pulloff, the loosely bound dextran could extend between the sample and the AFM probe surfaces and produce a second disengagement step as noted in the 2.0 h oxidation case (see Figure 7). The more "jagged" appearance of the retraction trace for the 1.0 h surface can be similarly interpreted. In this case, however, multiple dextran adsorption events occurred, or the AFM probe was released from adhesive interaction with dextran chains of varying length.[17] The mean adhesion force values (F_{adh}) shown in Table 1 were calculated from the negative deflection of the cantilever during the retraction step. Although the 2.0 h surface is an outlier, an overall trend is observed, namely, that the 0.5 and 4.0 h oxidized samples have similar adhesive characteristics as well as a proposed preponderance of grafted chains. It was also observed that the "jump to contact" (i.e., dip) of the AFM probe during approach occurred at larger distances for the 1.0 and 2.0 h surfaces than it did for the 0.5 and 4.0 h surfaces. This phenomenon is consistent with the presence of an "extended" dextran layer which increased the effective hydrated thickness of the 1.0 and 2.0 h surfaces. Conversely, the 0.5 and 4.0 h surfaces, because of their denser grafting to the substrate, gave rise to smaller "loops" which did not promote chain entanglement, and therefore appeared "thinner" in the aqueous environment in which the measurement was conducted. The jump to contact observed for the APTES surface occurred at an even greater distance. Nevertheless, it cannot be compared with the trends observed for the dextran surfaces because of the structural differences in the hydrated state of APTES and dextran.

To verify the hypothesis that loosely bound dextran detached from the 1.0 and 2.0 h surfaces, the AFM probe used in the force of adhesion measurements was analyzed by scanning electron microscopy (SEM). Imaging scans as well as composition maps comprise the analysis (data not shown) for the following elements: Si, O, N, and C. Also included in the study were as-received probes, as well as those cleaned with H_2SO_4/H_2O_2. The results indicated that the contamination from shipping material, primarily PDMS, on as-received probes is a serious consideration and that, furthermore, the cleaning procedure suggested by Lo et al.[11] is effective in eliminating contaminants. The SEM data obtained from AFM probes after the cleaning procedure were compared to the same probes after they were conditioned on the 1.0 and 2.0 h surfaces. The imaging data revealed the presence of ~200-nm-sized features near the apex of the probes. Furthermore, the carbon content on the surface of the probes increased dramatically after the adhesion measurements were performed, suggesting that the features observed

in the imaging scans were physisorbed dextran that was pulled off the surface during the retraction step of the adhesion measurements.

Conclusion

Controlling the $NaIO_4$ oxidation chemistry of dextran is a suitable approach to preparing biomimetic surfaces having varying grafting densities. As expected, the density of dextran features on the SiO_2 + APTES substrate decreased with increasing oxidation times and therefore increasing number of covalent bonds. The wettability data for the dextran modified surfaces was unexpected in that the shortest oxidation time surface, 0.5 h, exhibited the fastest rate and the largest extent of wetting. Aqueous AFM imaging afforded the roughness, height, diameter, and density analysis of dextran features. The data revealed that the 0.5 and 4.0 h surfaces had similar properties, while the 1.0 and 2.0 h surfaces behaved differently. These observations can tentatively be explained by considering that surfaces prepared with 0.5 h oxidized dextran resulted in complete coverage of the SiO_2 + APTES substrate. Upon preparation of the 1.0 and 2.0 h surfaces, however, oxidized dextran chains were not able to approach the amine-terminated substrate and, therefore, physisorbed onto the already covalently bound dextran. The force of adhesion data confirmed this hypothesis further, as was evidenced by the retraction trace of the force−distance curves. The multistep disengagements of the AFM probe from these surfaces are consistent with the presence of physisorbed dextran. Finally, because of the similarity between the 0.5 and 4.0 h surfaces, it was thought that the later one marked the onset of multilayer dextran formation.

Acknowledgment. We are grateful to the NIH for support through the following grants: NIH R01 HL60230, R01 HL67986, and T32 GM07612. We thank the NSF/MRSEC program, the Nanotechnology Initiative of Pennsylvania, and Penn Regional Nanotechnology Facility for assistance with AFM and SEM analyses, as well as the Rockefeller Brothers Fund.

References and Notes

(1) Cryer, A. *Biochemical Interactions at the Endothelium*; Elsevier: New York, 1983; pp 5−30.
(2) Dai, L.; St. John, H. A. W.; Bi, J.; Zientek, P.; Chatelier, R. C. *Surf. Interface Anal.* **2000**, *29*, 46−55.
(3) Hartley, P. G.; McArthur, S. L.; McLean, K. M.; Griesser, H. J. *Langmuir* **2002**, *18*, 2483−2494.
(4) Mason, M.; Vercruysse, K. P.; Kirker, K. R.; Frisch, R.; Marecak, D. M.; Prestwich, G. D.; Pitt, W. G. *Biomaterials* **2000**, *21*, 31−36.
(5) McArthur, S. L.; McLean, K. M.; Kingshott, P.; St. John, H. A. W.; Chatelier, R. C.; Griesser, H. J. *Colloids Surf., B* **2000**, *17*, 37−48.
(6) Elender, G.; Kuhner, M.; Sackmann, E. *Biosens. Bioelectron.* **1996**, *11*, 565−577.
(7) Pang, D.; Vidic, B.; Rodgers, J.; Berman, B. L.; Dritschilo, A. *Radiat. Oncol. Invest.* **1997**, 163−169.
(8) Wang, Y.; Song, R.; Li, Y.; Shen, J. *Surf. Sci.* **2003**, 136−148.
(9) Ditsent, V. E.; Skorokhodov, I. I.; Terenteva, N. A.; Zolotarev, M. N.; Belyakova, Z. V.; Belikova, Z. V. *Zh. Fiz. Khim.* **1976**, *50*, 1905−1906.
(10) Lin-Vien, D.; Colthup, N. B.; Fateley, W. B.; Grasselli, J. G. *The Handbook of Infrared and Raman Characteristic Frequencies*; Academic Press: Boston, 1991.
(11) Ek, S.; Iiskola, E. I.; Ninisto, L. *Langmuir* **2003**, *19*, 3461−3471.
(12) Hughes, G.; Nevell, T. P. *Trans. Faraday Soc.* **1948**, *44*, 941−948.
(13) Abdel-Magid, A. F.; Carson, K. G.; Harris, B. D.; Maryanoff, C. A.; Shah, R. D. *J. Org. Chem.* **1996**, *61*, 3849−3862.
(14) Hajos, A. *Studies in Organic Chemistry 1*; Elsevier Scientific Publishing: New York, 1979; pp 62−65.
(15) Lo, Y.; Huefner, N. D.; Chan, W. S.; Dryden, P.; Hagenhoff, B.; Beebe, T. P. *Langmuir* **1999**, *15*, 6522−6526.
(16) Dupont-Gillian, Ch. C.; Faurox, C. M. J.; Gardner, D. C. J.; Leggett, G. J. *J. Biomed. Mater. Res.* **2003**, *67A*, 548−558.
(17) Morra, M.; Cassineli, C.; Pavesio, A.; Renier, D. *J. Colloid Interface Sci.* **2003**, *259*, 236−243.
(18) *Digital Instruments. Guidelines for fluid operation with a MultiMode AFM*. Veeco Metrology Support Note No. 290, Rev. C; Veeco Instruments, 2004; pp 1−21.
(19) Senden, T. J.; Drummond, C. J. *Colloids Surf., A* **1995**, *94*, 29−51.
(20) Buist, G. J.; Hipperson, W. C. P.; Lewis, J. D. *J. Chem. Soc. A* **1969**, *2*, 307−312.
(21) Buist, G. J.; Bunton, C. A. *J. Chem. Soc., Abstr.* **1954**, 1406−1413.
(22) Crouthamel, C. E.; Hayes, A. M.; Martin, D. S. *J. Am. Chem. Soc* **1951**, *73*, 82−87.
(23) Rankl, M.; Laib, S.; Seeger, S. *Colloids Surf., B* **2003**, *30*, 177−186.
(24) Kurth, G. K.; Bein, T. *Langmuir* **1995**, *11*, 3061−3067.
(25) Andrade, J. D. *Polym. Sci. Technol.* **1986**, *34*, 29−40.
(26) Holly, F. J.; Refojo, M. F. *J. Biomed. Mater. Res.* **1975**, *9*, 315−326.
(27) Kuhner, M.; Sackmann, E. *Langmuir* **1996**, *12*, 4866−4876.
(28) Beyer, D.; Knoll, W.; Ringsdorf, H.; Elender, G.; Sackmann, E. *Trans. Faraday Soc.* **1996**, *284−285*, 825−828.
(29) Catalina, E. I.; Aberele, T.; Burchard, W. *Macromolecules* **2001**, *34*, 326−336.
(30) Hirata, Y.; Sano, Y.; Aoki, M.; Shohji, H.; Katoh, S.; Abe, J.; Hitsukuri, S.; Yamamoto, H. *Carbohydr. Polym.* **2003**, *53*, 331−335.

BM050601O